

GAUSSIAN SCENES: POSE-FREE SPARSE-VIEW SCENE RECONSTRUCTION USING DEPTH-ENHANCED DIFFUSION PRIORS

Soumava Paul, Prakhar Kaushik, Alan Yuille

CCVL, Johns Hopkins University

soumava2016@gmail.com, {pkaushil, ayuille}@jhu.edu

ABSTRACT

In this work, we introduce a generative approach for pose-free reconstruction of 360° scenes from a limited number of uncalibrated 2D images. Pose-free scene reconstruction from incomplete, unposed observations is usually regularized with depth estimation or 3D foundational priors. While recent advances have enabled sparse-view reconstruction of unbounded scenes with known camera poses using diffusion priors, these methods rely on explicit camera embeddings for extrapolating unobserved regions. This reliance limits their application in pose-free settings, where view-specific data is only implicitly available. To address this, we propose an instruction-following RGBD diffusion model designed to inpaint missing details and remove artifacts in novel view renders and depth maps of a 3D scene. We also propose a novel confidence measure for Gaussian representations to allow for better detection of these artifacts. By progressively integrating these novel views in a Gaussian-SLAM-inspired process, we achieve a multi-view-consistent Gaussian representation. Evaluations on the MipNeRF360 dataset demonstrate that our method surpasses existing pose-free techniques and performs competitively with state-of-the-art posed reconstruction methods in complex 360° scenes.

1 INTRODUCTION

Obtaining high-quality 3D reconstructions or novel views from a sparse set of images has been a long-standing goal in computer vision. Recent methods for sparse-view reconstruction often employ generative, geometric, or semantic priors to stabilize the optimization of NeRFs (Mildenhall et al., 2020) or Gaussian splats (Kerbl et al., 2023) in highly under-constrained scenarios. However, they typically assume access to accurate intrinsic and extrinsic parameters, often derived from dense observations. This reliance on ground-truth poses is a restrictive assumption, making these methods impractical for real-world applications. Moreover, pose estimation from sparse views is error-prone; both traditional Structure from Motion approaches and recent 3D foundational models (Wang et al., 2024; Leroy et al., 2024) struggle with insufficient matching features between image pairs. In response, recent pose-free approaches using 3D Gaussian splatting (3DGS) integrate monocular depth estimation (Ranftl et al., 2020), 2D semantic segmentation (Kirillov et al., 2023), or 3D foundational priors (Wang et al., 2024), optimizing 3D Gaussians and camera poses together during training. However, these methods are typically designed for scenes with high view overlap, and they often fail to reconstruct complex, large-scale 360° scenes with sparse coverage. Additionally, despite extensive regularization to prevent overfitting, the limited observations impede coherent synthesis of unobserved regions. This challenge underlines the need for additional generative regularization to enable accurate extrapolation and complete scene reconstruction.

Despite several previous attempts (Deng et al., 2022; Roessle et al., 2022; Li et al., 2024; Xiong et al., 2023; Zhu et al., 2023; Chung et al., 2023; Wang et al., 2023a; Jain et al., 2021; Niemeyer et al., 2022; Wynn and Turmukhambetov, 2023) in the field of sparse novel view synthesis, only a few - CF-3DGS (Fu et al., 2023), COGS Jiang et al. (2024), InstantSplat (Fan et al., 2024) have been successful in dealing with the problem without precomputed camera parameters. These methods jointly optimize Gaussians and camera parameters during training and use different 2D priors for

regularization. Although they find success in artifact and blur reduction, they are less effective in 360° scene reconstruction due to a lack of generative priors.

Reconstructing full 360° scenes from limited views requires robust priors, such as those from powerful 2D image or video diffusion models (Nichol et al., 2022; Ramesh et al., 2022; Saharia et al., 2022; Rombach et al., 2022) that encode common 3D structures. Recent methods (Liu et al., 2023; Sargent et al., 2024; Wu et al., 2024; Gao* et al., 2024; Blattmann et al., 2023) incorporate view and context conditioning into these models, fine-tuning them on extensive real-world and synthetic multi-view datasets to support radiance field optimization. This enables realistic extrapolation into unobserved areas of complex 360° scenes. However, these models depend on accurate pose information, making them unsuitable for scenarios where pose estimates deviate significantly from ground truth, leading to misaligned view generation. To our knowledge, only Gaussian Object (Yang et al., 2024), iFusion (Wu et al., 2023), and UpFusion (Nagoor Kani et al., 2024) provide pose-free generative solutions, but they are designed specifically for 3D object reconstruction, not large-scale scenes.

In the absence of camera conditioning, we augment Stable Diffusion Rombach et al. (2022) model with additional channels for context, 3DGS render, and depth maps with Gaussian artifacts, and a pixel-aligned confidence map capturing missing regions and reconstruction artifacts in the RGBD image. During inference, the model predicts a clean, inpainted version of the conditioning artifact image and an aligned depth map. This formulation prevents a pose-conditioning requirement common with most multiview diffusion models while also using limited multiview data for finetuning. This also alleviates dependency on large-scale 3D datasets which are usually synthetic and low quality compared to real-world scenes.

We present *GScenes*, an efficient method that uses 3D foundational (Leroy et al., 2024) and RGBD diffusion priors for pose-free sparse-view reconstruction of complex 360° scenes. We first estimate a point cloud and approximate scene intrinsics and extrinsics using DUST3R and then jointly optimize both Gaussians and camera parameters with just a few iterations of 3DGS. We then generate novel views by sampling from a B-spline trajectory fitted to the training views. Resulting renders and depth maps contain missing details and Gaussian artifacts that are refined by our diffusion prior and then used to further optimize the 3D Gaussians and camera poses. Despite using weaker generative priors compared to state-of-the-art pose-dependent methods, we show competitive qualitative and quantitative performance with ReconFusion (Wu et al., 2024) and CAT3D (Gao* et al., 2024) and comprehensively outperform all other pose-dependent and pose-free techniques on reconstruction quality. Our method leverages stronger priors than simple regularizers while not relying on million-scale multi-view data or huge compute resources to train a 3D-aware diffusion model.

In summary, our contributions are as follows.

- We propose a confidence measure to effectively detect empty regions, floaters, and artifacts in novel view renders and depth maps from 3DGS.
- We present an instruction-following RGBD diffusion model capable of synthesizing plausible novel views in a 3DGS scene initialized from sparse unposed images.
- We show that integrating our diffusion priors with a strong geometry prior in DUST3r facilitates fast reconstruction of a 3D scene previously only possible with pose-dependent finetuned video diffusion priors.
- We show that *GScenes* outperforms recent works based on regularization and generative priors in the reconstruction of large 3D scenes.

2 RELATED WORK

2.1 SPARSE-VIEW RADIANCE FIELDS

After NeRF Mildenhall et al. (2020) and 3D Gaussian Splatting Kerbl et al. (2023) advanced inverse rendering of radiance fields, numerous methods emerged to reduce dense scene capture needs to sparse views, categorized into regularization techniques and generalizable reconstruction priors.

Regularization Techniques Fitting a 3D representation from sparse observations is an ill-posed problem prone to local minima, often manifesting as 'floaters' in novel view renderings of radiance fields. Regularization techniques are commonly used to address limited data. Existing methods

leverage depth from Structure-from-Motion (SfM) [Deng et al. \(2022\)](#); [Roessle et al. \(2022\)](#), monocular estimation [Li et al. \(2024\)](#); [Xiong et al. \(2023\)](#); [Zhu et al. \(2023\)](#); [Chung et al. \(2023\)](#), or RGB-D sensors [Wang et al. \(2023a\)](#). DietNeRF [Jain et al. \(2021\)](#) uses a semantic consistency loss based on CLIP [Radford et al. \(2021\)](#) features, while FreeNeRF [Yang et al. \(2023\)](#) regularizes the frequency range of NeRF inputs. Approaching generative priors, RegNeRF [Niemeyer et al. \(2022\)](#) and DiffusioNeRF [Wynn and Turmukhambetov \(2023\)](#) maximize the likelihoods of rendered patches using normalizing flows or diffusion models, respectively.

Generalizable Reconstruction When only a few or a single view is available, regularization techniques are often insufficient to resolve reconstruction ambiguities. To address this, recent research focuses on training priors for novel view synthesis across multiple scenes. pixelNeRF [Yu et al. \(2021\)](#) uses pixel-aligned CNN features as conditioning for a shared NeRF MLP, while other approaches [Trevithick and Yang \(2021\)](#); [Chen et al. \(2021\)](#); [Henzler et al. \(2021\)](#); [Lin et al. \(2023b\)](#) condition NeRF on 2D or fused 3D features. Further priors have been learned on triplanes [Irshad et al. \(2023\)](#), voxel grids [Guo et al. \(2022\)](#), and neural points [Wewer et al. \(2023\)](#). Leveraging 3D Gaussian Splatting [Kerbl et al. \(2023\)](#), methods like pixelSplat [Charatan et al. \(2024\)](#) and MVSplat [Chen et al. \(2024\)](#) achieve state-of-the-art performance in stereo view interpolation and real-time rendering. However, these regression-based models often produce blurry outputs under high uncertainty. In contrast, generative methods like GeNVS [Chan et al. \(2023\)](#) and latentSplat [Wewer et al. \(2024\)](#) aim to sample from multi-modal distributions, offering better handling of ambiguous novel views.

Generative Priors For ambiguous novel views, predicting expectations over all reconstructions may be unreliable. Consequently, regression approaches fall short, whereas generative methods attempt to sample from a multi-modal distribution.

Diffusion Models In recent years, diffusion models [Ho et al. \(2020\)](#); [Dhariwal and Nichol \(2021\)](#) emerged as the state-of-the-art for image synthesis. They are characterized by a pre-defined forward noising process that gradually destroys data by adding random (typically Gaussian) noise. The objective is to learn a reverse denoising process with a neural network that, after training, can sample from the data distribution given pure noise. Important improvements include refined sampling procedures [Song et al. \(2021\)](#); [Karras et al. \(2022\)](#) and the more efficient application in a spatially compressed latent space compared to the high-resolution pixel space [Rombach et al. \(2022\)](#). Their stable optimization, in contrast to GANs, enabled today’s text-to-image generators [Nichol et al. \(2022\)](#); [Ramesh et al. \(2022\)](#); [Saharia et al. \(2022\)](#); [Rombach et al. \(2022\)](#) trained on billions of images [Schuhmann et al. \(2022\)](#). In recent years, diffusion models [Ho et al. \(2020\)](#); [Dhariwal and Nichol \(2021\)](#) have become state-of-the-art for image synthesis. These models use a forward noising process to progressively add random (typically Gaussian) noise, and train a neural network to reverse this process, enabling sampling from the data distribution given pure noise. Key improvements include refined sampling techniques [Song et al. \(2021\)](#); [Karras et al. \(2022\)](#) and more efficient application in compressed latent spaces rather than high-resolution pixel spaces [Rombach et al. \(2022\)](#). Their stable optimization, unlike GANs, has enabled the success of text-to-image generators [Nichol et al. \(2022\)](#); [Ramesh et al. \(2022\)](#); [Saharia et al. \(2022\)](#); [Rombach et al. \(2022\)](#) trained on billions of images [Schuhmann et al. \(2022\)](#).

2D Diffusion for 3D While diffusion models have been applied directly on 3D representations like triplanes [Shue et al. \(2023\)](#); [Chen et al. \(2023a\)](#), voxel grids [Müller et al. \(2023\)](#), or (neural) point clouds [Zhou et al. \(2021\)](#); [Melas-Kyriazi et al. \(2023\)](#); [Schröppel et al. \(2024\)](#), 3D data is scarce. Given the success of large-scale diffusion models for image synthesis, there is a great research interest in leveraging them as priors for 3D reconstruction and generation. DreamFusion [Poole et al. \(2023\)](#) and follow-ups [Wang et al. \(2023b\)](#); [Lin et al. \(2023a\)](#); [Chen et al. \(2023b\)](#); [Deng et al. \(2023\)](#); [Tang et al. \(2024\)](#) employ score distillation sampling (SDS) to iteratively maximize the likelihood of radiance field renderings under a conditional 2D diffusion prior. For sparse-view reconstruction, existing approaches incorporate view-conditioning via epipolar feature transform [Zhou and Tulsiani \(2023\)](#), cross-attention to encoded relative poses [Liu et al. \(2023\)](#); [Sargent et al. \(2024\)](#), or pixelNeRF [Yu et al. \(2021\)](#) feature renderings [Wu et al. \(2024\)](#). However, this fine-tuning is expensive and requires large-scale multi-view data, which we circumvent with *GScenes*.

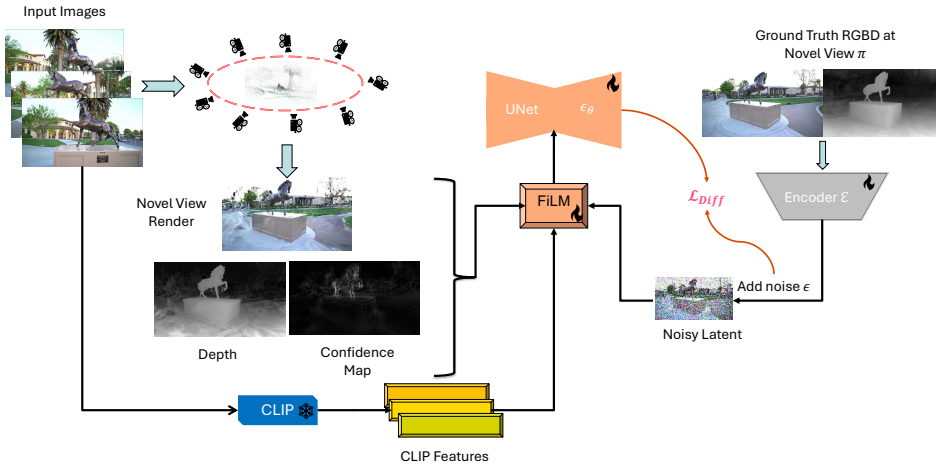


Figure 1: **Overview of *GScenes***. We render 3D Gaussians fitted to our sparse set of M views from a novel viewpoint. The resulting render and depth map have missing regions and Gaussian artifacts, which are rectified by an RGBD image-to-image diffusion model. This then acts as pseudo ground truth to spawn and update 3D Gaussians and satisfy the new view constraints. This process is repeated for several novel views spanning the 360° scene until the representation becomes multi-view consistent.

3 METHOD

This section begins with an overview of our pipeline in Sec 3.1. In Sec 3.3, we present a confidence measure for 3DGS rasterization to capture artifacts and missing regions in rendered images and depth maps. We detail the different components of our generative prior in Sec 3.2 and the subsequent 3DGS optimization in Sec 3.4. We end the section with a final pose alignment step for a given set of test views in Sec 3.5.

3.1 ALGORITHM OVERVIEW

Problem Setup Given a set of M images $\mathcal{I} = \{I_1, I_2, \dots, I_M\}$ of an underlying 3D scene with unknown intrinsics and extrinsics, our goal is to reconstruct the 3D scene, estimate the camera poses of a monocular camera at the M training views, and synthesize novel views at evaluation time given by N unseen test images $\{I_{M+1}, I_{M+2}, \dots, I_{M+N}\}$.

Algorithm 1 *GScenes* Algorithm

Require: Sparse input image set $\mathcal{I} = \{I_1, I_2, \dots, I_M\}$
Ensure: Set of 3D Gaussians \mathcal{G} and camera poses $\pi = \{\pi_1, \pi_2, \dots, \pi_M\}$

- 1: $\hat{\mathcal{I}} \leftarrow \mathcal{I}$
- 2: $\mathcal{G} \leftarrow$ Optimize 3DGS with DUS3r point cloud for $1k$ iterations
- 3: **for** N iterations **do**
- 4: $\pi \leftarrow$ Sample novel camera pose.
- 5: $\mathbf{I}, \mathbf{D} \leftarrow R_\pi(\mathcal{G})$ - Render from camera π
- 6: $\mathbf{I} \leftarrow$ Refine(\mathbf{I})
- 7: $\hat{\mathbf{I}} \leftarrow \hat{\mathbf{I}} \cup \{\mathbf{I}\}$
- 8: $\mathcal{G} \leftarrow$ Optimize 3DGS for k iterations
- 9: **end for**

An overview of our method is given in Fig 1 and Alg 1. We initialize *GScenes* with an incomplete dense Gaussian point cloud reconstruction from sparse input images using InstantSplat Fan et al. (2024). We use this incomplete Gaussian scene representation as an implicit geometric prior and sample novel views along a smooth B-spline trajectory fitted to training views. We use our customized RGBD diffusion prior to generate plausible novel views. In addition to CLIP features of source

images for context, we devise a novel 3DGS confidence measure to effectively guide our diffusion model towards empty regions and potential artifacts in a novel view render. We then run $10k$ iterations of 3DGS optimization, sampling a novel view before each densification step (Fu et al., 2023) to obtain our final scene representation.

Gaussian Point Cloud Initialization The DUST3r pipeline gives us a pixel-aligned dense-stereo point cloud $\mathbf{P} \in \mathbb{R}^{S \times 3}$, camera intrinsics $\{\mathbf{K}_i \in \mathbb{R}^{3 \times 3}\}_{i=1}^M$ and extrinsics $\{\mathbf{E}_i = [\mathbf{R}_i | \mathbf{T}_i]\}_{i=1}^M$ for our M input images. Nevertheless, both \mathbf{P} and the estimated poses demonstrate sub-optimal alignment compared to those generated by COLMAP (Schönberger and Frahm, 2016) from the dense observation dataset. Consequently, similar to the approach used in InstantSplat, we start by initializing 3D Gaussians at each location within the globally aligned point cloud \mathbf{P} . Subsequently, we jointly optimize both the Gaussian attributes and camera parameters over the course of $1k$ iterations without incorporating any form of Adaptive Density Control.

3.2 RGBD DIFFUSION PRIORS FOR NVS

Despite the initial geometric prior, many areas of the scene remain unobserved due to the sparsity of the input set, leading to areas of no Gaussians (0-Gaussians) in the 3D representation \mathcal{G} obtained from *InstantSplat* and zero opacity regions, floaters, and artifacts in novel views. Regularization techniques or 3D foundational priors cannot help with inferring missing details, prompting us to develop an instruction-following RGBD diffusion model comprising a variational autonecoder with encoder \mathcal{E} , decoder \mathcal{D} and UNet ϵ_θ operating in the latent space of the VAE. ϵ_θ learns to predict noise in a noisy latent z_t conditioned on a RGBD image \hat{I} , corresponding confidence map \mathcal{C} , clip conditioning c_{clip} , and a text instruction y . \hat{I} and \mathcal{C} are obtained by rendering \mathcal{G} from novel views.

We initialize ϵ_θ with the pretrained weights of the Stable-Diffusion-2 checkpoint (Rombach et al., 2022) to leverage its image generation capabilities for RGBD image-to-image synthesis. We introduce additional channels in the first convolutional layer of ϵ_θ to support image conditioning with \hat{I} . Specifically, we concatenate z_t , $\mathcal{E}(\hat{I})$ and $\hat{\mathcal{C}}$, where $\hat{\mathcal{C}}$ is \mathcal{C} downsampled to the resolution of the latent space. Weights of all newly added channels are initialized to zero. However, conditioning on \hat{I} and \mathcal{C} alone does not ensure novel view synthesis coherent with the observed inputs. In the absence of explicit 3D conditioning, we augment our generative model with scene context using CLIP features. We extract CLIP features $c_{clip} \in \mathcal{R}^{M \times d}$ of the M training images to modulate intermediate feature layers in ϵ_θ . However, instead of the usual cross-attention mechanism, we resort to a more parameter-efficient approach by using Feature-wise Linear Modulation (FiLM) layers (Perez et al., 2018). These layers work by generating scaling and shifting parameters for the UNet feature maps, allowing c_{clip} to modulate intermediate activations in the UNet. We first pass c_{clip} through trainable self-attention modules to capture shared semantic information across views and create a unified, context-aware representation.

$$c_{attn} = \text{SelfAttention}(c_{clip}) \quad (1)$$

$c_{attn} \in \mathcal{R}^d$ is next passed through layer-specific fully connected layers to predict scale and shift parameters γ, β as:

$$\gamma^{(l)}, \beta^{(l)} = FC^{(l)}(c_{attn}) \quad (2)$$

Let $\mathbf{F}^{(l)} \in \mathcal{R}^{k \times h \times w}$ represent a feature map in ϵ_θ at a layer l , where k is the number of channels, h and w are the spatial dimensions. The FiLM modulation is applied element-wise as:

$$\mathbf{F}_{mod}^{(l)} = \text{FiLM}(\mathbf{F}^{(l)} | \gamma^{(l)}, \beta^{(l)}) = \gamma^{(l)} \cdot \mathbf{F}^{(l)} + \beta^{(l)} \quad (3)$$

This conditioning enables the dynamic adaptation of the UNet’s feature maps facilitated by scale and shift parameters conditioned on the CLIP embedding, thereby directing the UNet’s output to align with the semantic features captured by CLIP. We implement FiLM modulation with CLIP embeddings exclusively within the down and mid blocks of the UNet, as this approach allows for

the effective integration of conditional information without perturbing the generation process in the up(sample) blocks.

3.3 PIXEL-ALIGNED CONFIDENCE MAP

To effectively guide our diffusion model towards recognizing and repairing artifacts in novel views, we design a novel pixel-aligned confidence measure based on the cumulative transmittance along a viewing direction at a pixel i and the number of overlapping Gaussians at that pixel. Formally, we define confidence at a pixel as:

$$\mathcal{C}_i = -\log(T_i + \epsilon) \times n_{contrib} \quad (4)$$

where $T_i = \prod_i (1 - \alpha_i)$ represents the fraction of light transmitted through pixel i without interaction and $n_{contrib}$ is the number of contributing 3D Gaussians. $\epsilon > 0$ is a small constant to prevent taking the logarithm of 0. Intuitively, low T_i means the viewing ray interacts significantly with 3D Gaussians, implying higher confidence in the pixel’s color. The negative logarithm provides a more perceptually uniform confidence scale. $n_{contrib}$ further increases (or decreases) the reliability of the rendered color or depth due to consensus among multiple (few) Gaussian primitives.

To the best of our knowledge, only 3DGS-Enhancer (Liu et al., 2024) proposes a confidence measure based on alpha-compositing of Gaussian scales, assuming that well-reconstructed areas are represented by Gaussians of small volumes, whereas large scales usually point towards artifacts. However, as can be seen in Fig 2, this assumption does not hold true in the case of regions with monotonous textures, which do not necessarily need multiple Gaussians of small scales to represent fine details. One can clearly see that our proposed measure effectively captures both empty regions as well as reconstruction artifacts, avoiding false positives unlike Liu et al. (2024).

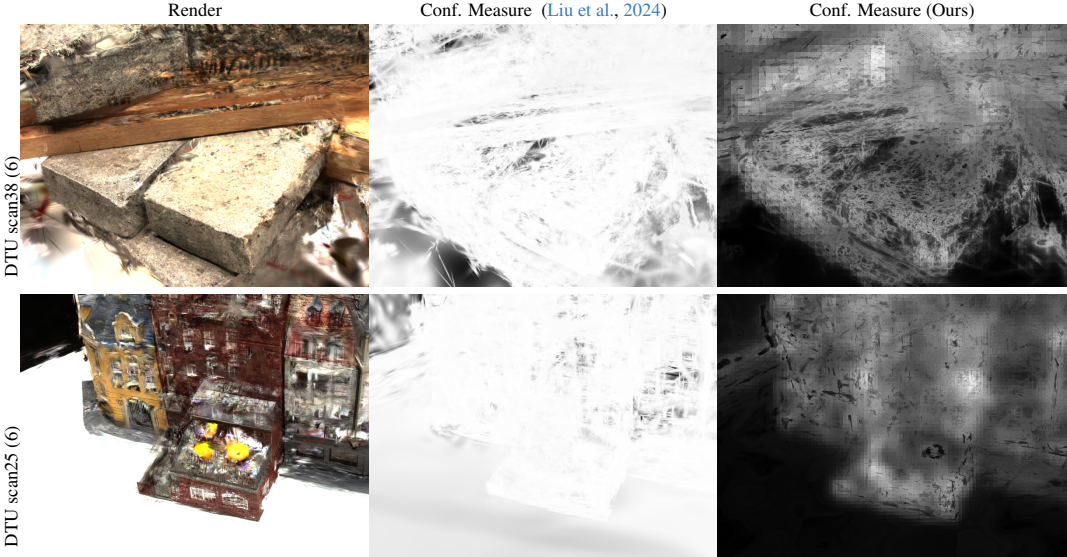


Figure 2: Confidence Measure comparison with 3DGS-Enhancer (Liu et al., 2024). Our confidence map accurately identifies artifacts and 0-Gaussian regions in the image (darker pixels) while (Liu et al., 2024) incorrectly attributes high confidence to regions with overlap of small-scale Gaussians.

3.3.1 SYNTHETIC RGBD DATASET CREATION

For training the additional weights in ϵ_θ for RGBD image-to-image diffusion, we rely on a set $\mathcal{X} = \{(I^i, \hat{I}^i, C^i, y^i)_{i=1}^N\}$ of data quartets, each containing a clean RGBD image I^i , an RGBD image with artifacts \hat{I}^i and the corresponding confidence map C^i , and an edit instruction for fine-tuning y^i , to “teach” the diffusion model how to detect Gaussian artifacts guided by the confidence map and

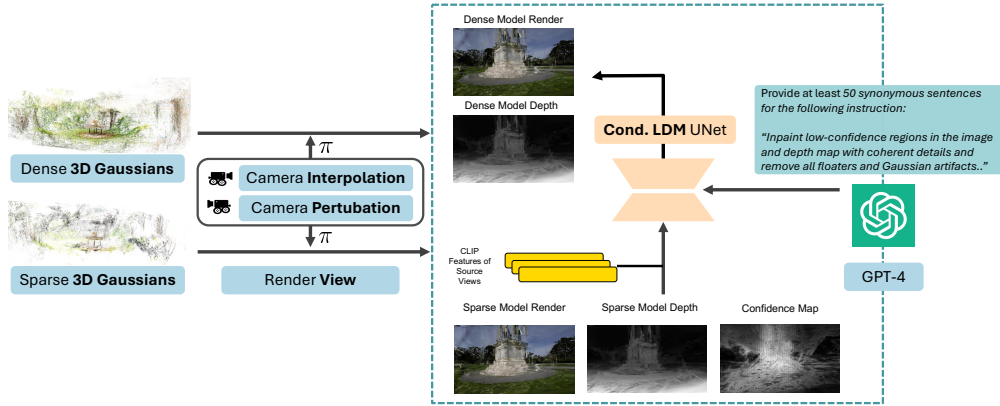


Figure 3: **Training our RGBD diffusion model.** Pairs of RGBD clean images and images with artifacts are obtained from 3DGS fitted to sparse and dense observations, respectively, across 165 scenes. CLIP features provide scene context, and a confidence map additionally detects empty regions and artifacts in the artifact image. These are combined with one of 51 synonymous prompts generated by GPT-4 Achiam et al. (2023) from a base instruction. The Stable Diffusion UNet is then fine-tuned with a dataset of 28, 161 samples.

generate a clean version of the conditioning image. For this, we build an *artifact simulation engine* comprising a high-quality 3DGS model fitted to dense views, a low-quality 3DGS model fitted to few views, and camera interpolation and perturbation modules to use supervision of the high-quality model at viewpoints beyond ground truth camera poses. The fine-tuning setup is illustrated in Fig. 3. For a given scene, we fit sparse models for $M \in \{3, 6, 9, 18\}$ number of views. To have diversity in edit instructions, we start with a base human-intuitive instruction - “Inpaint low-confidence regions in the image and depth map with coherent details and remove all floaters and Gaussian artifacts.” and ask GPT-4 to generate 50 synonymous instructions. During training, each image triplet is randomly combined with one of these 51 instructions. Additionally, for each M , we save the CLIP features c_{clip} of the M sparse views for conditioning ϵ_θ .

3.3.2 DEPTH-AUGMENTED AUTOENCODER FINETUNING

For encoding and decoding RGBD images, we customize a Variational AutoEncoder by introducing additional channels in the first and last convolutional layers of the Stable Diffusion VAE. A similar approach was followed by Stan et al. (2023), where their KL-autencoder was finetuned with triplets containing RGB images, depth maps, and captions to train the weights in the new channels. However, the depth maps used for fine-tuning this VAE were estimated using MiDaS(Ranftl et al., 2020), which are usually blurry monocular depth estimates. As such, reconstructing RGBD images using this VAE produces depth maps with extreme blur - not ideal for a scene reconstruction problem. Hence, we further finetune this VAE with our synthetic dataset, which contains depth maps rendered by the differentiable 3DGS rasterizer, giving accurate pixel depth with high-frequency details. Specifically, we use the following objective:

$$\begin{aligned}
 \mathcal{L}_{\text{autoencoder}} = & \min_{\mathcal{E}, D} \max_{D_\psi} (\mathcal{L}_{\text{rec}}(x, D(\mathcal{E}(x))) \\
 & - \mathcal{L}_{\text{adv}}(D(\mathcal{E}(x))) \\
 & + \log(D_\psi(x)) \\
 & + \mathcal{L}_{\text{reg}}(x; \mathcal{E}, D))
 \end{aligned} \tag{5}$$

where \mathcal{L}_{rec} is a combination of L1, perceptual losses for the RGB channels, and Pearson Correlation Coefficient (PCC), TV regularization losses for the depth channels. \mathcal{L}_{adv} is the adversarial loss, D_ψ is a patch-based discriminator loss, and \mathcal{L}_{reg} is the KL-regularisation loss. The incorporation of PCC and TV terms for the depth channels leads to better retention of high-frequency details in the reconstructed depth map, as observed in Fig 4. We finetune this VAE on a subset of our dataset for 5000 training steps with batch size 16 and learning rate 1e-05.

3.3.3 UNET FINETUNING

With our finetuned autoencoder, we next train the UNet with the frozen VAE on \mathcal{X} with the following objective:

$$\mathcal{L} = \mathbb{E}_{i \sim \mathcal{U}(N), \epsilon \sim \mathcal{N}(\mathbf{0}, \mathbf{I}), t} \left[\|\epsilon_t - \epsilon_{\theta}(\mathbf{z}_t^i; t, \mathcal{E}(\hat{I}), \hat{\mathcal{C}}, c_{attn}, c_{\theta}(y^i))\|_2^2 \right] \quad (6)$$

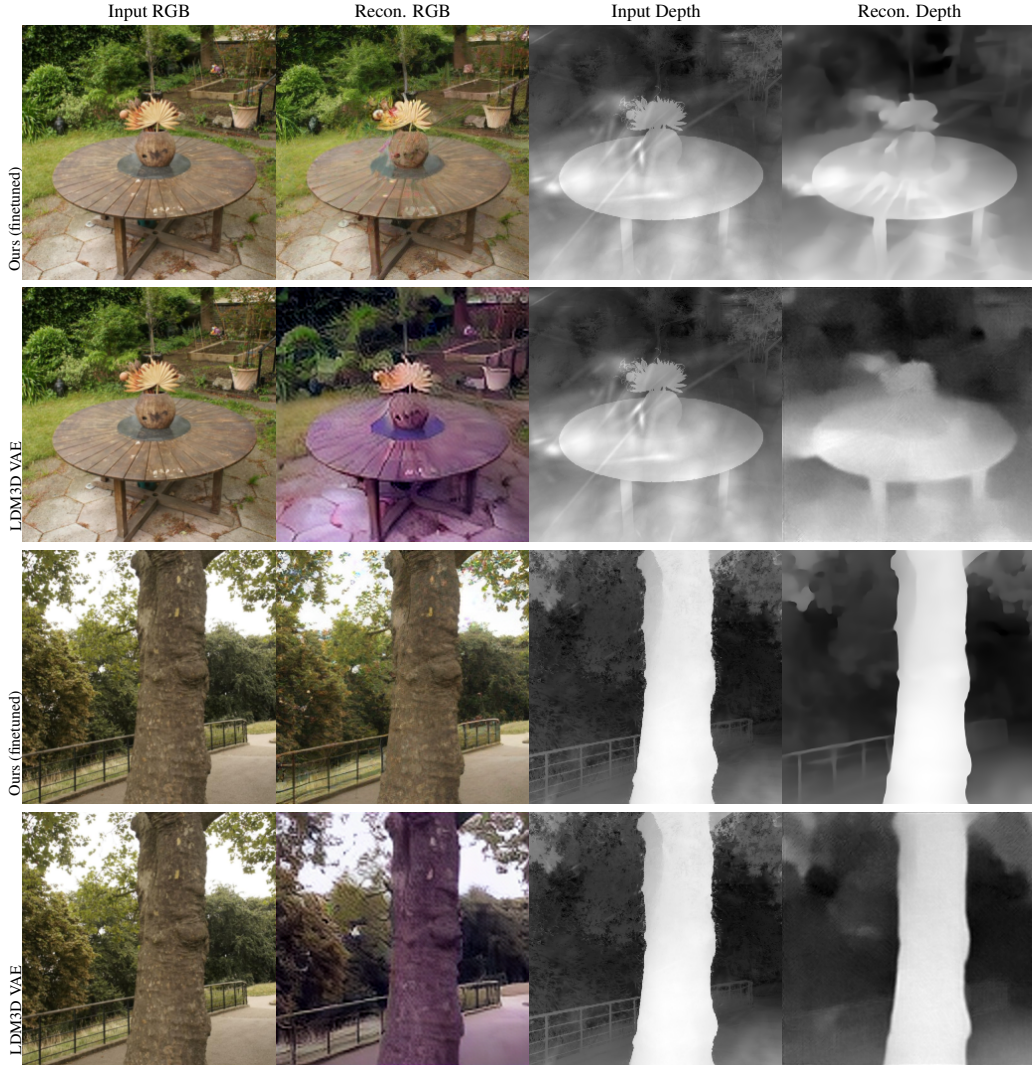


Figure 4: RGBD reconstruction comparison of our finetuned VAE with the LDM3D VAE (Stan et al., 2023). Unlike LDM3D, our VAE finetuned on a synthetic dataset preserves sharp details and edges of the input depth map while also preventing color artifacts in RGB.

where \mathbf{z}_t^i is the encoded image I^i diffused with sampled noise ϵ at time step t . Thus, the UNet learns to generate clean RGBD images I^i , conditioned on artifact RGBD images I^i , confidence maps \mathcal{C}^i , CLIP features c_{attn} , and instructions y^i .

3.3.4 INFERENCE USING RGBD NOVEL VIEW SYNTHESIS

At inference time, given a render and depth map with artifacts and the base instruction $y =$ “Inpaint low-confidence regions in the image and depth map with coherent details and remove all floaters

and Gaussian artifacts." the finetuned UNet ϵ_θ learns to predict the noise in latent \mathbf{z}_t according to $t \sim \mathcal{U}[t_{min}, t_{max}]$ as:

$$\hat{\epsilon}_t = \epsilon_\theta(\mathbf{z}_t; t, \emptyset, \hat{\mathcal{C}}, c_{attn}, \emptyset) + s_I(\epsilon_\theta(\mathbf{z}_t; t, \mathcal{E}(\hat{I}), \hat{\mathcal{C}}, c_{attn}, \emptyset) - \epsilon_\theta(\mathbf{z}_t; t, \emptyset, \hat{\mathcal{C}}, c_{attn}, \emptyset)) \\ + s_T(\epsilon_\theta(\mathbf{z}_t; t, \emptyset, \hat{\mathcal{C}}, c_{attn}, c_\theta(y)) - \epsilon_\theta(\mathbf{z}_t; t, \mathcal{E}(\hat{I}), \hat{\mathcal{C}}, c_{attn}, \emptyset)) \quad (7)$$

where s_I and s_T are the RGBD image and prompt guidance scales, dictating how strongly the final multistep reconstruction agrees with the RGBD render \hat{I} and the edit prompt y , respectively. After $k = 20$ DDIM Song et al. (2021) sampling steps, we obtain our final RGBD render by decoding the denoised latent as $x_\pi = [I_\pi, D_\pi] = \mathcal{D}(z_0)$.

3.4 SCENE RECONSTRUCTION WITH DIFFUSION PRIORS

Our diffusion priors infer plausible detail in unobserved regions. However, the generated images at novel poses lack 3D consistency due to lack of explicit 3D conditioning of the UNet through pose embeddings. For this, we devise an iterative strategy where we first sample novel views along a B-spline trajectory fitted to the training views. We initialize the Gaussian optimization with the set of Gaussians \mathcal{G} fitted to the training views. Each novel view is added to the training stack at the beginning of every densification step to encourage the optimization to adjust to the distilled scene priors. At every iteration, we sample either an observed or unobserved viewpoint from the current training stack. We jointly optimize Gaussian attributes, and both train and novel poses. We employ the 3DGS objective for the training views. For novel views, we employ the SparseFusion Zhou and Tulsiani (2023) objective in the RGB space (Wu et al., 2024) and a PCC loss for the rendered and denoised depths.

$$\mathcal{L}_{sample}(\psi) = \mathbb{E}_{\pi, t} \left[w(t) (\|I_\pi - \hat{I}_\pi\|_1 + \mathcal{L}_p(I_\pi, \hat{I}_\pi)) \right] + w_d \cdot PCC(D_\pi, \hat{D}_\pi) \quad (8)$$

where \mathcal{L}_p is the perceptual loss Zhang et al. (2018), $w(t)$ a noise-dependent weighting function, I_π, D_π are the rendered image and depth at novel viewpoint π , and \hat{I}_π, \hat{D}_π are their rectified versions obtained with our diffusion prior.

3.5 TEST-TIME POSE ALIGNMENT

GScenes reconstructs a plausible 3D scene from unposed source images. However, reconstruction with few views is inherently ambiguous as several solutions can satisfy the train view constraints. Hence, the reconstructed scene would most likely be quite different from the actual scene from which M views were sampled. Hence, for a given set of test views, following prior work Fan et al. (2024); Jiang et al. (2024), we freeze the Gaussian attributes and optimize the camera pose for each target view by minimizing a photometric loss between the rendered image and test view. Following this alignment step performed for 500 iterations per test image, we evaluate the NVS quality.

4 EXPERIMENTS

We compare *GScenes* with state-of-the-art pose-free and pose-required sparse-view reconstruction methods in Fig and Table . We also ablate the different components and design choices of our diffusion model.

4.1 EXPERIMENTAL SETUP

Evaluation Dataset We evaluate *GScenes* on the 9 scenes of the MipNeRF360 dataset (Barron et al., 2022), comprising 5 outdoor and 4 indoor scenes. Each scene has a central object or area of complex geometry with an equally intricate background. This makes it the most challenging 360° dataset compared to CO3D (Reizenstein et al., 2021), RealEstate 10K (Zhou et al., 2018), DTU (Jensen et al., 2014), etc. We pick the M -view splits as proposed by ReconFusion Wu et al. (2024) and CAT3D Gao* et al. (2024) and evaluate all baselines on the official test views where every 8th image is held out for testing.

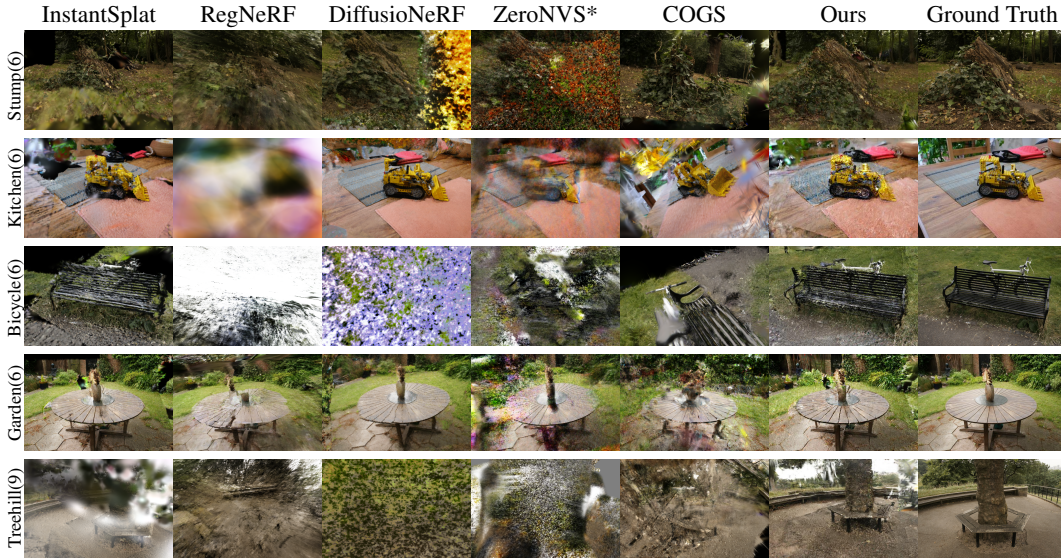


Figure 5: **Qualitative comparison** of GScenes with few-view methods. Our approach consistently fares better in recovering image structure from foggy geometry, where baselines typically struggle with “floaters” and color artifacts.

Fine-tuning Dataset We fine-tune our diffusion model on a mix of 165 scenes encompassing Tanks and Temples (Knapitsch et al., 2017), CO3D (Reizenstein et al., 2021), DTU (Jensen et al., 2014), Deep Blending (Hedman et al., 2018), and LLFF (Mildenhall et al., 2019) to obtain a total of 28161 data samples. We first train 3DGS on sparse and dense subsets of each scene for $M \in \{3, 6, 9, 18\}$. For $M > 18$, novel view renders and depth maps mostly show Gaussian blur as artifacts. Finetuning this model takes about 1-day on a single A6000 GPU.

Metrics Our quantitative metrics are used to evaluate two tasks - quality of novel views post reconstruction and camera pose estimation. For the former, we compute 3 groups of metrics - FID (Heusel et al., 2017) and KID (Bińkowski et al., 2018) due to the generative nature of our approach, perceptual metrics LPIPS (Zhang et al., 2018) and DISTS (Ding et al., 2020) to measure similarity in image structure and texture in the feature space, and pixel-aligned metrics PSNR and SSIM. However, PSNR and SSIM are not suitable evaluators of generative techniques (Chan et al., 2023; Sargent et al., 2024) as they favor pixel-aligned blurry estimates over high-frequency details.

Baselines We compare our approach against 8 baselines. FreeNeRF (Yang et al., 2023), RegNeRF (Niemeyer et al., 2022), DiffusioNeRF (Wynn and Turmukhambetov, 2023) are pose-required few-view regularization methods based on NeRFs. ZeroNVS (Sargent et al., 2024) reconstructs a complete 3D scene from a single image using a novel camera normalization scheme and anchored SDS loss. We use the ZeroNVS* baseline introduced in ReconFusion (Wu et al., 2024), designed to adapt ZeroNVS to multi-view inputs. ReconFusion and CAT3D are state-of-the-art multi-view conditioned diffusion models for sparse-view reconstruction. We use the reported average performance on the 9 scenes of MipNeRF360 with classical metrics - PSNR, SSIM, and LPIPS for quantitative comparison and pick the relevant scenes and test views from the two papers for qualitative comparison. For pose-free methods, we pick InstantSplat (Fan et al., 2024) and COGS (Jiang et al., 2024) and show that our approach outperforms both in NVS qualitatively and quantitatively.

4.2 IMPLEMENTATION DETAILS

We implement our entire framework in PyTorch 2.3.1 and run all experiments on single A5000 or A6000 GPUs. We render images and depth maps in the 400-600 pixel range as this is closest to the output resolution of Stable Diffusion. We finetuned our diffusion model for $10k$ iterations with batch size 16 and learning rate $1e-4$. To enable classifier-free guidance, we randomly dropout conditioning inputs like text, image, confidence map, etc., with probability of 0.05 during training.

We fit 3D Gaussians to sparse input images and a DUST3r point cloud and train it for $1k$ iterations as in Fan et al. (2024) to obtain our initial Gaussian representation \mathcal{G} . The classifier-free guidance

scales are set to $s_I = 2.5$ and $s_T = 7.5$. We use $t_{max} = 0.99$ and linearly decrease t_{min} from 0.98 to 0.70. We sample novel-view renders and depth maps for $k = 20$ DDIM sampling steps. w_d is decayed linearly from 1 to 0.01. We also linearly decay the weight of \mathcal{L}_{sample} from 1 to 0.1 over $10k$ iterations. *GScenes* reconstructs the complete 3D scene in about 5 minutes on a single A6000 GPU.

4.3 COMPARISON RESULTS

Table 1: **Quantitative comparison** with state-of-the-art sparse-view reconstruction techniques on classical metrics.

| Method | PSNR \uparrow | | | SSIM \uparrow | | | LPIPS \downarrow | | |
|----------------|-----------------|--------|--------|-----------------|--------|--------|--------------------|--------|--------|
| | 3-view | 6-view | 9-view | 3-view | 6-view | 9-view | 3-view | 6-view | 9-view |
| FreeNeRF | 11.888 | 12.877 | 13.680 | 0.146 | 0.180 | 0.197 | 0.675 | 0.654 | 0.638 |
| RegNeRF | 12.297 | 13.209 | 13.802 | 0.147 | 0.170 | 0.180 | 0.668 | 0.656 | 0.625 |
| DiffusioNeRF | 13.134 | 16.191 | 16.732 | 0.167 | 0.283 | 0.337 | 0.680 | 0.543 | 0.530 |
| ZeroNVS* | 11.902 | 11.789 | 11.729 | 0.142 | 0.133 | 0.128 | 0.710 | 0.702 | 0.694 |
| ReconFusion | 15.50 | 16.93 | 18.19 | 0.358 | 0.401 | 0.432 | 0.585 | 0.544 | 0.511 |
| CAT3D | 16.62 | 17.72 | 18.67 | 0.377 | 0.425 | 0.460 | 0.515 | 0.482 | 0.460 |
| InstantSplat | 13.657 | 14.733 | 14.926 | 0.222 | 0.265 | 0.246 | 0.603 | 0.540 | 0.590 |
| COGS | 12.267 | 12.428 | 13.030 | 0.173 | 0.186 | 0.201 | 0.616 | 0.632 | 0.596 |
| <i>GScenes</i> | 14.976 | 15.972 | 16.563 | 0.284 | 0.295 | 0.314 | 0.593 | 0.517 | 0.577 |

Table 2: **Quantitative comparison** with few-view reconstruction techniques on metrics suited for generative reconstruction.

| Method | FID \downarrow | | | KID \downarrow | | | DISTS \downarrow | | |
|----------------|------------------|---------|---------|------------------|--------|--------|--------------------|--------|--------|
| | 3-view | 6-view | 9-view | 3-view | 6-view | 9-view | 3-view | 6-view | 9-view |
| FreeNeRF | 342.484 | 343.378 | 334.805 | 0.252 | 0.262 | 0.268 | 0.376 | 0.363 | 0.357 |
| RegNeRF | 343.593 | 335.606 | 325.228 | 0.260 | 0.276 | 0.257 | 0.387 | 0.383 | 0.371 |
| DiffusioNeRF | 323.047 | 269.995 | 246.265 | 0.230 | 0.166 | 0.141 | 0.395 | 0.325 | 0.328 |
| ZeroNVS* | 356.395 | 350.362 | 343.930 | 0.283 | 0.294 | 0.299 | 0.433 | 0.427 | 0.413 |
| InstantSplat | 268.526 | 226.110 | 242.853 | 0.191 | 0.131 | 0.140 | 0.294 | 0.298 | 0.310 |
| COGS | 231.274 | 274.827 | 248.220 | 0.136 | 0.183 | 0.152 | 0.288 | 0.310 | 0.286 |
| <i>GScenes</i> | 253.659 | 220.292 | 210.255 | 0.176 | 0.098 | 0.106 | 0.284 | 0.245 | 0.241 |

We report qualitative and quantitative comparisons of *GScenes* against all related baselines in Fig 5 and Tables 1 and 2. Out of the 8 baselines, only *InstantSplat* and *COGS* are pose-free techniques, while the remaining require ground truth poses for both training and evaluation. Note that *COGS* relies on ground truth camera intrinsics while *GScenes* and *InstantSplat* do not. On the classical metrics (Tab 1), we are third behind the 2 SOTA posed reconstruction methods - *CAT3D* and *ReconFusion*. Except for FID and KID on the 3-view split, we outperform all related baselines in Table 2. Due to the unavailability of open-source code, evaluating *ReconFusion* and *CAT3D* on these measures is unfortunately not possible.

4.4 ABLATION STUDIES

In Fig 6, we ablate different components of our diffusion model. We pick the *counter* and *treehill* scenes for this experiment. The *Base* variant only performs image-to-image diffusion in the RGB space and tries to fill in missing details and remove artifacts based on the partial information available from the novel view render. Conditioning with our pixel-aligned confidence measure leads to better detection and elimination of Gaussian artifacts. Foreground and background artifacts in both the render and depth map are not effectively dealt with in the absence of this conditioning input. Performing diffusion only in the RGB space usually produces depth maps with sharp foreground artifacts. Incorporating joint modeling of RGB and depth through our RGBD diffusion model and subsequent depth optimization during scene reconstruction (Sec 3.4) produces smoother depth maps while also restricting floaters and Gaussian artifacts. As we randomly dropout conditioning prompts

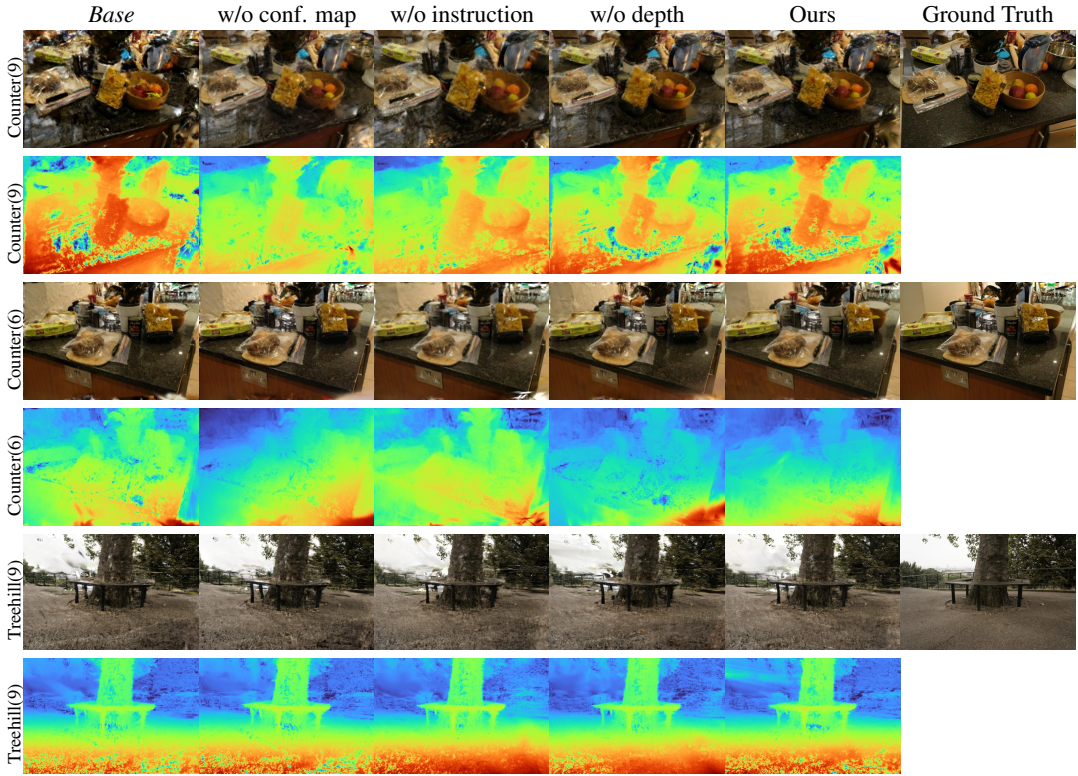


Figure 6: Ablation Study with the *Counter* and *Treehill* scenes of MipNeRF360. Images above are heldout test-view renders obtained after test-time pose alignment (Sec 3.5). All of our proposed conditionings improve the diffusion model’s ability to inpaint missing details and remove artifacts in novel view renders.

(instruction, confidence map, etc.) during fine-tuning, the diffusion model is adept at image synthesis even in the absence of the base instruction prompt. However, an intuitive instruction like “Inpaint low-confidence regions in the image and depth map with coherent details and remove all floaters and Gaussian artifacts.” usually guides the model better in localizing empty regions and Gaussian artifacts.

Table 3: **Pose estimation accuracy with *GScenes***. SfM-poses for training views estimated from the full observation set are used as ground truth. We report errors in camera rotation and translation using Absolute Trajectory Error (ATE) and Relative Pose Error (RPE) as in [Bian et al. \(2023\)](#). Despite the DUST3r initialization of camera extrinsics and subsequent pose optimization, there are large errors w.r.t COLMAP poses of the dense observation set, harming test-pose alignment and subsequent NVS quality.

| | 3-view | RPE _t ↓ | | 3-view | RPE _r ↓ | | 3-view | ATE ↓ | |
|----------------|--------|--------------------|--------|---------|--------------------|--------|--------|--------|--------|
| | | 6-view | 9-view | 6-view | 9-view | 9-view | | 6-view | 9-view |
| <i>GScenes</i> | 37.684 | 27.893 | 30.916 | 124.501 | 58.915 | 40.424 | 0.261 | 0.294 | 0.266 |

4.5 LIMITATIONS & FUTURE WORK

GScenes is a first step towards a generative solution for pose-free sparse-view reconstruction of large complex scenes. However, it is not free of its fair share of limitations. The quality of the final reconstruction depends heavily on the initial relative pose estimation by the DUST3r pipeline, and even though the poses are further optimized jointly with Gaussian attributes during training, there

are still large differences with the ground truth COLMAP poses estimated from dense views as we show in Tab 3. This limits fair comparison with posed reconstruction methods, as even the test-time pose alignment step (Sec 3.5) cannot compensate for the initial errors in the pipeline. Finally, our diffusion model is limited in its 3D outpainting abilities as, unlike a simplified 2-view setting, there is no explicit view conditioning possible in a general pose-free N-view setting. Existing state-of-the-art posed reconstruction techniques like ReconFusion and CAT3D are able to leverage stronger diffusion priors for scene reconstruction as the diffusion models have view conditioning in the form of pixelNeRF embeddings or “raymap” representations. We hope to address some of these limitations as part of our future work.

5 CONCLUSION

In this work, we present *GScenes* where we integrate an instruction-following RGBD diffusion model with a pose-free reconstruction pipeline in InstantSplat to reconstruct a 360° 3D scene from a few uncalibrated 2D images. We also introduce a pixel-aligned confidence measure to further guide the diffusion model in uncertain regions with missing details and artifacts. Our experiments show that *GScenes* outperforms existing pose-free reconstruction methods in scene reconstruction and performs competitively with state-of-the-art posed sparse-view reconstruction methods.

REFERENCES

- Josh Achiam, Steven Adler, Sandhini Agarwal, Lama Ahmad, Ilge Akkaya, Florencia Leoni Aleman, Diogo Almeida, Janko Altenschmidt, Sam Altman, Shyamal Anadkat, et al. Gpt-4 technical report. In *arXiv*, 2023. 7
- Jonathan T. Barron, Ben Mildenhall, Dor Verbin, Pratul P. Srinivasan, and Peter Hedman. Mip-nerf 360: Unbounded anti-aliased neural radiance fields. In *CVPR*, 2022. 9
- Wenjing Bian, Zirui Wang, Kejie Li, Jiawang Bian, and Victor Adrian Prisacariu. Nope-nerf: Optimising neural radiance field with no pose prior. 2023. 12
- Mikołaj Bińkowski, Dougal J. Sutherland, Michael Arbel, and Arthur Gretton. Demystifying MMD GANs. In *ICLR*, 2018. 10
- Andreas Blattmann, Tim Dockhorn, Sumith Kulal, Daniel Mendelevitch, Maciej Kilian, Dominik Lorenz, Yam Levi, Zion English, Vikram Voleti, Adam Letts, Varun Jampani, and Robin Rombach. Stable video diffusion: Scaling latent video diffusion models to large datasets, 2023. 2
- Eric R. Chan, Koki Nagano, Matthew A. Chan, Alexander W. Bergman, Jeong Joon Park, Axel Levy, Miika Aittala, Shalini De Mello, Tero Karras, and Gordon Wetzstein. GeNVS: Generative novel view synthesis with 3D-aware diffusion models. In *ICCV*, 2023. 3, 10
- David Charatan, Sizhe Li, Andrea Tagliasacchi, and Vincent Sitzmann. pixelsplat: 3d gaussian splats from image pairs for scalable generalizable 3d reconstruction. In *CVPR*, 2024. 3
- Anpei Chen, Zexiang Xu, Fuqiang Zhao, Xiaoshuai Zhang, Fanbo Xiang, Jingyi Yu, and Hao Su. Mvsnerf: Fast generalizable radiance field reconstruction from multi-view stereo. In *ICCV*, 2021. 3
- Hansheng Chen, Jiatao Gu, Anpei Chen, Wei Tian, Zhuowen Tu, Lingjie Liu, and Hao Su. Single-stage diffusion nerf: A unified approach to 3d generation and reconstruction. In *ICCV*, 2023a. 3
- Rui Chen, Yongwei Chen, Ningxin Jiao, and Kui Jia. Fantasia3d: Disentangling geometry and appearance for high-quality text-to-3d content creation. In *ICCV*, 2023b. 3
- Yuedong Chen, Haofei Xu, Chuanxia Zheng, Bohan Zhuang, Marc Pollefeys, Andreas Geiger, Tat-Jen Cham, and Jianfei Cai. Mvsplat: Efficient 3d gaussian splatting from sparse multi-view images. 2024. 3
- Jaeyoung Chung, Jeongtaek Oh, and Kyoung Mu Lee. Depth-regularized optimization for 3d gaussian splatting in few-shot images. In *arXiv*, 2023. 1, 3
- Congyue Deng, Chiyu Jiang, Charles R Qi, Xinchun Yan, Yin Zhou, Leonidas Guibas, Dragomir Anguelov, et al. Nerdi: Single-view nerf synthesis with language-guided diffusion as general image priors. In *CVPR*, 2023. 3
- Kangle Deng, Andrew Liu, Jun-Yan Zhu, and Deva Ramanan. Depth-supervised NeRF: Fewer views and faster training for free. In *CVPR*, 2022. 1, 3

-
- Prafulla Dhariwal and Alexander Nichol. Diffusion models beat gans on image synthesis. In *NeurIPS*, 2021. 3
- Keyan Ding, Kede Ma, Shiqi Wang, and Eero P Simoncelli. Image quality assessment: Unifying structure and texture similarity. In *IEEE TPAMI*, 2020. 10
- Zhiwen Fan, Wenyan Cong, Kairun Wen, Kevin Wang, Jian Zhang, Xinghao Ding, Danfei Xu, Boris Ivanovic, Marco Pavone, Georgios Pavlakos, Zhangyang Wang, and Yue Wang. Instantsplat: Unbounded sparse-view pose-free gaussian splatting in 40 seconds. In *arXiv*, 2024. 1, 4, 9, 10
- Yang Fu, Sifei Liu, Amey Kulkarni, Jan Kautz, Alexei A. Efros, and Xiaolong Wang. Colmap-free 3d gaussian splatting. 2023. 1, 5
- Ruiqi Gao*, Aleksander Holynski*, Philipp Henzler, Arthur Brussee, Ricardo Martin-Brualla, Pratul P. Srinivasan, Jonathan T. Barron, and Ben Poole*. Cat3d: Create anything in 3d with multi-view diffusion models. *arXiv*, 2024. 2, 9
- Pengsheng Guo, Miguel Angel Bautista, Alex Colburn, Liang Yang, Daniel Ulbricht, Joshua M. Susskind, and Qi Shan. Fast and explicit neural view synthesis. In *WACV*, 2022. 3
- Peter Hedman, Julien Philip, True Price, Jan-Michael Frahm, George Drettakis, and Gabriel Brostow. Deep blending for free-viewpoint image-based rendering. In *ACM TOG*, 2018. 10
- Philipp Henzler, Jeremy Reizenstein, Patrick Labatut, Roman Shapovalov, Tobias Ritschel, Andrea Vedaldi, and David Novotny. Unsupervised learning of 3d object categories from videos in the wild. In *CVPR*, 2021. 3
- Martin Heusel, Hubert Ramsauer, Thomas Unterthiner, Bernhard Nessler, and Sepp Hochreiter. Gans trained by a two time-scale update rule converge to a local nash equilibrium. In *NeurIPS*, 2017. 10
- Jonathan Ho, Ajay Jain, and Pieter Abbeel. Denoising diffusion probabilistic models. In *NeurIPS*, 2020. 3
- Muhammad Zubair Irshad, Sergey Zakharov, Katherine Liu, Vitor Guizilini, Thomas Kollar, Adrien Gaidon, Zsolt Kira, and Rares Ambrus. Neo 360: Neural fields for sparse view synthesis of outdoor scenes. In *ICCV*, 2023. 3
- Ajay Jain, Matthew Tancik, and Pieter Abbeel. Putting nerf on a diet: Semantically consistent few-shot view synthesis. In *ICCV*, 2021. 1, 3
- Rasmus Jensen, Anders Dahl, George Vogiatzis, Engil Tola, and Henrik Aanæs. Large scale multi-view stereopsis evaluation. In *CVPR*, 2014. 9, 10
- Kaiwen Jiang, Yang Fu, Mukund Varma T, Yash Belhe, Xiaolong Wang, Hao Su, and Ravi Ramamoorthi. A construct-optimize approach to sparse view synthesis without camera pose. *SIGGRAPH*, 2024. 1, 9, 10
- Tero Karras, Miika Aittala, Timo Aila, and Samuli Laine. Elucidating the design space of diffusion-based generative models. In *NeurIPS*, 2022. 3
- Bernhard Kerbl, Georgios Kopanas, Thomas Leimkühler, and George Drettakis. 3d gaussian splatting for real-time radiance field rendering. In *ACM TOG*, 2023. 1, 2, 3
- Alexander Kirillov, Eric Mintun, Nikhila Ravi, Hanzi Mao, Chloe Rolland, Laura Gustafson, Tete Xiao, Spencer Whitehead, Alexander C. Berg, Wan-Yen Lo, Piotr Dollár, and Ross Girshick. Segment anything. *arXiv:2304.02643*, 2023. 1
- Arno Knapitsch, Jaesik Park, Qian-Yi Zhou, and Vladlen Koltun. Tanks and temples: benchmarking large-scale scene reconstruction. In *ACM TOG*, 2017. 10
- Vincent Leroy, Yohann Cabon, and Jerome Revaud. Grounding image matching in 3d with mast3r, 2024. 1, 2
- Jiahe Li, Jiawei Zhang, Xiao Bai, Jin Zheng, Xin Ning, Jun Zhou, and Lin Gu. Dngaussian: Optimizing sparse-view 3d gaussian radiance fields with global-local depth normalization. In *CVPR*, 2024. 1, 3
- Chen-Hsuan Lin, Jun Gao, Luming Tang, Towaki Takikawa, Xiaohui Zeng, Xun Huang, Karsten Kreis, Sanja Fidler, Ming-Yu Liu, and Tsung-Yi Lin. Magic3d: High-resolution text-to-3d content creation. In *CVPR*, 2023a. 3
- Kai-En Lin, Lin Yen-Chen, Wei-Sheng Lai, Tsung-Yi Lin, Yi-Chang Shih, and Ravi Ramamoorthi. Vision transformer for nerf-based view synthesis from a single input image. In *WACV*, 2023b. 3
- Ruoshi Liu, Rundi Wu, Basile Van Hoorick, Pavel Tokmakov, Sergey Zakharov, and Carl Vondrick. Zero-1-to-3: Zero-shot one image to 3d object. In *ICCV*, 2023. 2, 3

-
- Xi Liu, Chaoyi Zhou, and Siyu Huang. 3dgs-enhancer: Enhancing unbounded 3d gaussian splatting with view-consistent 2d diffusion priors. *arXiv preprint arXiv:2410.16266*, 2024. 6
- Luke Melas-Kyriazi, Christian Rupprecht, and Andrea Vedaldi. Pc2: Projection-conditioned point cloud diffusion for single-image 3d reconstruction. In *CVPR*, 2023. 3
- Ben Mildenhall, Pratul P. Srinivasan, Rodrigo Ortiz-Cayon, Nima Khademi Kalantari, Ravi Ramamoorthi, Ren Ng, and Abhishek Kar. Local light field fusion: Practical view synthesis with prescriptive sampling guidelines. In *ACM TOG*, 2019. 10
- Ben Mildenhall, Pratul P. Srinivasan, Matthew Tancik, Jonathan T. Barron, Ravi Ramamoorthi, and Ren Ng. Nerf: Representing scenes as neural radiance fields for view synthesis. In *ECCV*, 2020. 1, 2
- Norman Müller, Yawar Siddiqui, Lorenzo Porzi, Samuel Rota Buló, Peter Kotschieder, and Matthias Nießner. Diffrf: Rendering-guided 3d radiance field diffusion. In *CVPR*, 2023. 3
- Bharath Raj Nagoor Kani, Hsin-Ying Lee, Sergey Tulyakov, and Shubham Tulsiani. Upfusion: Novel view diffusion from unposed sparse view observations. In *European Conference on Computer Vision (ECCV)*, 2024. 2
- Alexander Quinn Nichol, Prafulla Dhariwal, Aditya Ramesh, Pranav Shyam, Pamela Mishkin, Bob McGrew, Ilya Sutskever, and Mark Chen. GLIDE: Towards photorealistic image generation and editing with text-guided diffusion models. In *ICML*, 2022. 2, 3
- Michael Niemeyer, Jonathan T. Barron, Ben Mildenhall, Mehdi S. M. Sajjadi, Andreas Geiger, and Noha Radwan. Regnerf: Regularizing neural radiance fields for view synthesis from sparse inputs. In *CVPR*, 2022. 1, 3, 10
- Ethan Perez, Florian Strub, Harm de Vries, Vincent Dumoulin, and Aaron C. Courville. Film: Visual reasoning with a general conditioning layer. In *AAAI*, 2018. 5
- Ben Poole, Ajay Jain, Jonathan T. Barron, and Ben Mildenhall. Dreamfusion: Text-to-3d using 2d diffusion. In *ICLR*, 2023. 3
- Alec Radford, Jong Wook Kim, Chris Hallacy, Aditya Ramesh, Gabriel Goh, Sandhini Agarwal, Girish Sastry, Amanda Askell, Pamela Mishkin, Jack Clark, et al. Learning transferable visual models from natural language supervision. In *ICML*, 2021. 3
- Aditya Ramesh, Prafulla Dhariwal, Alex Nichol, Casey Chu, and Mark Chen. Hierarchical text-conditional image generation with clip latents. In *arXiv*, 2022. 2, 3
- René Ranftl, Katrin Lasinger, David Hafner, Konrad Schindler, and Vladlen Koltun. Towards robust monocular depth estimation: Mixing datasets for zero-shot cross-dataset transfer. In *IEEE TPAMI*, 2020. 1, 7
- Jeremy Reizenstein, Roman Shapovalov, Philipp Henzler, Luca Sbordone, Patrick Labatut, and David Novotny. Common objects in 3d: Large-scale learning and evaluation of real-life 3d category reconstruction. In *ICCV*, 2021. 9, 10
- Barbara Roessle, Jonathan T. Barron, Ben Mildenhall, Pratul P. Srinivasan, and Matthias Nießner. Dense depth priors for neural radiance fields from sparse input views. In *CVPR*, 2022. 1, 3
- Robin Rombach, Andreas Blattmann, Dominik Lorenz, Patrick Esser, and Björn Ommer. High-resolution image synthesis with latent diffusion models. In *CVPR*, 2022. 2, 3, 5
- Chitwan Saharia, William Chan, Saurabh Saxena, Lala Li, Jay Whang, Emily L Denton, Kamyar Ghasemipour, Raphael Gontijo Lopes, Burcu Karagol Ayan, Tim Salimans, Jonathan Ho, David J Fleet, and Mohammad Norouzi. Photorealistic text-to-image diffusion models with deep language understanding. In *NeurIPS*, 2022. 2, 3
- Kyle Sargent, Zizhang Li, Tanmay Shah, Charles Herrmann, Hong-Xing Yu, Yunzhi Zhang, Eric Ryan Chan, Dmitry Lagun, Li Fei-Fei, Deqing Sun, and Jiajun Wu. ZeroNVS: Zero-shot 360-degree view synthesis from a single real image. In *CVPR*, 2024. 2, 3, 10
- Johannes Lutz Schönberger and Jan-Michael Frahm. Structure-from-motion revisited. In *CVPR*, 2016. 5
- Philipp Schröppel, Christopher Wewer, Jan Eric Lenssen, Eddy Ilg, and Thomas Brox. Neural point cloud diffusion for disentangled 3d shape and appearance generation. In *CVPR*, 2024. 3

-
- Christoph Schuhmann, Romain Beaumont, Richard Vencu, Cade Gordon, Ross Wightman, Mehdi Cherti, Theo Coombes, Aarush Katta, Clayton Mullis, Mitchell Wortsman, Patrick Schramowski, Srivatsa Kundurthy, Katherine Crowson, Ludwig Schmidt, Robert Kaczmarczyk, and Jenia Jitsev. Laion-5b: An open large-scale dataset for training next generation image-text models. In *NeurIPS*, 2022. 3
- J. Ryan Shue, Eric Ryan Chan, Ryan Po, Zachary Anknor, Jiajun Wu, and Gordon Wetzstein. 3d neural field generation using triplane diffusion. In *CVPR*, 2023. 3
- Jiaming Song, Chenlin Meng, and Stefano Ermon. Denoising diffusion implicit models. In *ICLR*, 2021. 3, 9
- Gabriela Ben Melech Stan, Diana Wofk, Scottie Fox, Alex Redden, Will Saxton, Jean Yu, Estelle Aflalo, Shao-Yen Tseng, Fabio Nonato, Matthias Muller, and Vasudev Lal. Ldm3d: Latent diffusion model for 3d, 2023. 7, 8
- Jiaxiang Tang, Jiawei Ren, Hang Zhou, Ziwei Liu, and Gang Zeng. Dreamgaussian: Generative gaussian splatting for efficient 3d content creation. In *ICLR*, 2024. 3
- Alex Trevithick and Bo Yang. Grf: Learning a general radiance field for 3d scene representation and rendering. In *ICCV*, 2021. 3
- Guangcong Wang, Zhaoxi Chen, Chen Change Loy, and Ziwei Liu. Sparsenerf: Distilling depth ranking for few-shot novel view synthesis. In *ICCV*, 2023a. 1, 3
- Haochen Wang, Xiaodan Du, Jiahao Li, Raymond A Yeh, and Greg Shakhnarovich. Score jacobian chaining: Lifting pretrained 2d diffusion models for 3d generation. In *CVPR*, 2023b. 3
- Shuzhe Wang, Vincent Leroy, Yohann Cabon, Boris Chidlovskii, and Jerome Revaud. Dust3r: Geometric 3d vision made easy. In *CVPR*, 2024. 1
- Christopher Wewer, Eddy Ilg, Bernt Schiele, and Jan Eric Lenssen. SimNP: Learning self-similarity priors between neural points. In *ICCV*, 2023. 3
- Christopher Wewer, Kevin Raj, Eddy Ilg, Bernt Schiele, and Jan Eric Lenssen. latentsplat: Autoencoding variational gaussians for fast generalizable 3d reconstruction. In *arXiv*, 2024. 3
- Chin-Hsuan Wu, Yen-Chun Chen, Bolivar Solarte, Lu Yuan, and Min Sun. ifusion: Inverting diffusion for pose-free reconstruction from sparse views. *arXiv preprint arXiv:2312.17250*, 2023. 2
- Rundi Wu, Ben Mildenhall, Philipp Henzler, Keunhong Park, Ruiqi Gao, Daniel Watson, Pratul P. Srinivasan, Dor Verbin, Jonathan T. Barron, Ben Poole, and Aleksander Holynski. Reconfusion: 3d reconstruction with diffusion priors. In *CVPR*, 2024. 2, 3, 9, 10
- Jamie Wynn and Daniyar Turmukhambetov. DiffusioNeRF: Regularizing Neural Radiance Fields with Denoising Diffusion Models. In *CVPR*, 2023. 1, 3, 10
- Haolin Xiong, Sairisheek Muttukuru, Rishi Upadhyay, Pradyumna Chari, and Achuta Kadambi. Sparseggs: Real-time 360° sparse view synthesis using gaussian splatting. In *arXiv*, 2023. 1, 3
- Chen Yang, Sikuang Li, Jiemin Fang, Ruofan Liang, Lingxi Xie, Xiaopeng Zhang, Wei Shen, and Qi Tian. Gaussianobject: High-quality 3d object reconstruction from four views with gaussian splatting. *ACM Transactions on Graphics*, 2024. 2
- Jiawei Yang, Marco Pavone, and Yue Wang. Freenerf: Improving few-shot neural rendering with free frequency regularization. In *CVPR*, 2023. 3, 10
- Alex Yu, Vickie Ye, Matthew Tancik, and Angjoo Kanazawa. pixelNeRF: Neural radiance fields from one or few images. In *CVPR*, 2021. 3
- Richard Zhang, Phillip Isola, Alexei A Efros, Eli Shechtman, and Oliver Wang. The unreasonable effectiveness of deep features as a perceptual metric. In *CVPR*, 2018. 9, 10
- Linqi Zhou, Yilun Du, and Jiajun Wu. 3d shape generation and completion through point-voxel diffusion. In *ICCV*, 2021. 3
- Tinghui Zhou, Richard Tucker, John Flynn, Graham Fyffe, and Noah Snavely. Stereo magnification: Learning view synthesis using multiplane images. In *SIGGRAPH*, 2018. 9
- Zhizhuo Zhou and Shubham Tulsiani. Sparsefusion: Distilling view-conditioned diffusion for 3d reconstruction. In *CVPR*, 2023. 3, 9
- Zehao Zhu, Zhiwen Fan, Yifan Jiang, and Zhangyang Wang. Fsgs: Real-time few-shot view synthesis using gaussian splatting. In *arXiv*, 2023. 1, 3